Grain boundary segregation and precipitation in an Al-Zn-Mg-Cu alloy

Huan Zhao [1], Baptiste Gault [1,2], Frédéric De Geuser[3], Dirk Ponge [1], Dierk Raabe [1]*

1. Max-Planck-Institut für Eisenforschung, Max-Planck-Str. 1, 40237, Düsseldorf, Germany
2. Department of Materials, Royal School of Mines, Imperial College, Exhibition Road, London SW7 2AZ, United Kingdom
3. Univ. Grenoble Alpes, CNRS, Grenoble INP, SIMaP, F-38000 Grenoble, France

Abstract. High strength Al-alloys are highly susceptible to intergranular embrittlement, which severely limits their lifetime. This article summarizes our recent work on the effect of solute segregation in the precipitation behavior at grain boundaries (GBs) compared to the grain interiors. Solute segregation could accelerate the precipitation behavior at GBs, which causes the formation of coarse precipitates and precipitate free zones along GBs. Furthermore, the interplay of solute segregation and the local structure at GBs has been considered. We show that the distinct segregation and precipitation behavior occurs within the same GB, which makes the GB excess of solutes at one facet significantly higher than the other facet. This paper enriches the current understanding on the role of chemistry and structure at GBs related to intergranular fracture and corrosion resistance in high strength Al-alloys.

1 Introduction

7xxx Al-alloys are widely employed in aerospace and automobile applications due to their low mass density and high strength ability since Sander and Meissner's findings in 1923 [1-3]. 7xxx series are alloyed with small amounts of Zn and Mg (Al-Zn-Mg system) or Zn, Mg and Cu (Al-Zn-Mg-Cu system). These alloys are mainly strengthened through precipitation hardening by forming nano-sized precipitates during aging, which further act as obstacles impeding dislocation motion [4]. 7xxx Al-alloys have a high nucleation rate of precipitates among the precipitation-hardening Al-alloys, which provide high specific strength. The precipitation behavior of Al-Zn-Mg-(Cu) alloys has been well studied and established as the sequence of the supersaturated solid solution to Guinier-Prestion (GP) zones, followed by metastable η' phases and stable η phases ($MgZn_2$) [5-7].

For many age-hardened Al-alloys, the precipitation reaction starts with the formation of coherent, nano-sized GP zones as found in the early work of Guinier and Preston [8, 9]. GP zones transform to metastable, semi-coherent η' precipitates during aging. η' phase has the hexagonal Laves structure with a lattice parameter of a=b=0.496 nm, c=1.402 nm [10, 11]. η' precipitates occur as plates on {111} planes of the Al-matrix, elongated along the <110> direction. The composition of η' precipitates is controversial in literature due to their metastability. The previous results show that they contain 30-40 at.% Zn, ~33 at.% Mg, 5-10 at.% Cu and balance Al, with variations on the alloy composition and aging treatment [7, 12, 13]. The η'-plates eventually transform to coarse, incoherent η phases during over-aging, accompanied by a decrease in strength. The equilibrium η phase can also heterogeneously nucleate at GBs, phase boundaries, and dislocations during quenching [14]. The η phase has a similar hexagonal Laves structure with the lattice parameter of a=0.5221 nm, c=0.8567 nm [5, 15, 16]. It is originally proposed that the chemical composition of the η phase is $MgZn_2$. While, it has been widely shown that Cu and/or Al atoms substitute some of the Zn sites and cause the chemical composition to $Mg(Zn,Al)_2$ for Al-Zn-Mg system and $Mg(Zn,Al,Cu)_2$ for Al-Zn-Mg-Cu system [7].

Despite the wide commercial applications of 7xxx Al-alloys, their usage is restricted by the resistance to stress corrosion cracking and intergranular embrittlement [17-20]. For this purpose, they are often used in a slightly overaged temper to provide better corrosion resistance while at a loss in strength. The embrittlement has been attributed to the formation of coarse, incoherent precipitates along GBs [21-23], as well as the precipitate-free zones (PFZs) adjacent to GBs [24, 25]. GBs differ in structure and properties from the grain interiors, which could cause solute segregation according to the Gibbs adsorption isotherm. Such equilibrium segregation phenomenon modifies the GB composition compared to the bulk, which can play an important role in the early stage precipitation and PFZ formation at GBs [26-30]. An experimental investigation on the details regarding

* Corresponding author: h.zhao@mpie.de

segregation and its influence on the precipitation behavior at GBs is required. Besides, there is a strong motivation to understand more about the basic aspects of the interplay between chemistry and local structure at GBs, which is essential in understanding the local segregation and precipitation behavior. In this article, we have reviewed our recent work in the application of atom probe, in conjunction with electron microscopy, electron backscatter diffraction to study the segregation and precipitation behavior in an Al-Zn-Mg-Cu alloy.

2 Experimental

The studied Al-Zn-Mg-Cu alloy was laboratory-cast and homogenized in a vacuum induction furnace. Table 1 summarizes the material's chemical composition measured by the wet chemical analysis. The homogenized ingot was then subsequently hot-rolled at 450 °C and solution heat-treated for 1 hour at 475 °C by water quenching. The as-quenched samples were immediately aged at 120ºC for different time to follow the aging response according to the Vickers hardness measurements. Electron backscatter diffraction (EBSD) was used to locate high-angle GBs. Atom probe tomography (APT) specimens were then prepared from the GBs using a FEI Helios Plasma Focused Ion Beam (Plasma FIB) instrument with a Xe source. APT probing was conducted on a local electrode atom probe (LEAP 5000XS), under ultra-high vacuum conditions of 10^{-11} Torr with a 20% pulse fraction and a 250 kHz pulse rate, at a cryogenic temperature of 40 K. APT datasets were analyzed using the commercial software package IVAS 3.8.4. The reconstruction parameters were calibrated according to the crystallographic poles appearing on the detector hit map. Scanning transmission electron microscopy (STEM) characterization was performed on a spherical probe corrected FEI Titan Themis 60-300 STEM, operated at 300 keV. High angle annular dark field (HAADF) images, bright field (BF)-STEM were recorded.

Table 1. Chemical composition of an Al-Zn-Mg-Cu alloy

Alloy	Zn	Mg	Cu	Zr	Fe	Si	Al
(wt.%)	6.22	2.46	2.13	0.15	0.02	<0.01	rest

3. Results and discussions

3.1 Precipitation in the bulk

Fig. 1 shows the hardness curve from the as-quenched state (120±3 HV) to the peak aged state (185±5 HV) and further to the overaged state (171±3 HV). Representative APT analysis over the aging response are also shown insets, with iso-surfaces of 10 at.% Zn highlighting the Zn-Mg-rich precipitates [31]. Over the first 2 hours aging at 120 ºC, nearly spherical Zn-Mg-rich zones with a high number density of 10^{24}–10^{25} m^{-3} form and develop into GP zones. The composition of the precipitates is approximately 75 at. % Al, 13 at. % Zn, 10 at. % Mg and 2 at. % Cu. 120°C for 24 hours aging produced the peak hardness. The overaged state was conducted by further aging the peak aged sample at a higher temperature of 180°C for 6 hours. Significant precipitate coarsening is investigated in the overaged state, which decreases the hardness.

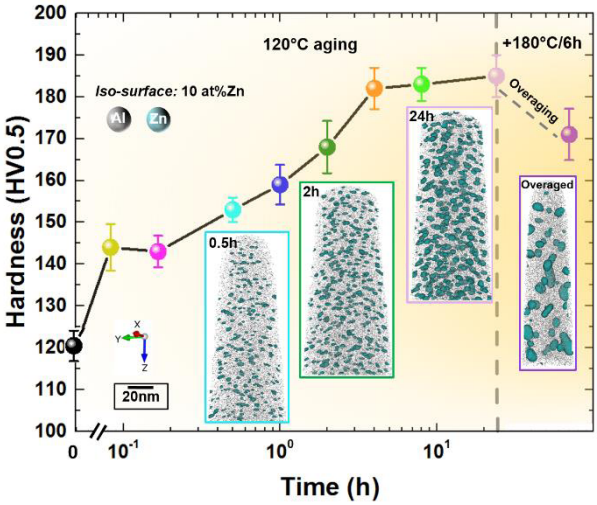

Fig. 1. Evolution of the hardness over the course of aging. Insets are APT analysis of the precipitates highlighted by 10 at. % Zn. (Reprinted with permission from Ref. 31)

3.2 Comparison of APT samples of Al-alloys prepared by Ga-FIB and Xe-FIB

We have then turned our attention to investigate the segregation effect on the precipitation behavior at GBs by APT. The site-specific APT specimen was commonly prepared by the lift-out method using a FEI focused ion beam with Ga+ source. This can become problematic for Al-alloys in the GB segregation study due to the fast diffusion of Ga in Al. Fig. 2 shows one representative example of the APT specimen of the peak aged Al-Zn-Mg-Cu alloy prepared on a Ga-FIB. The GB is visualized by the depletion of all solutes but the strong enrichment of Ga, while the GP zones are clearly shown in the adjacent bulk. This evidences that the presence of Ga during FIB preparation affects the precise quantification of solute segregation at GBs.

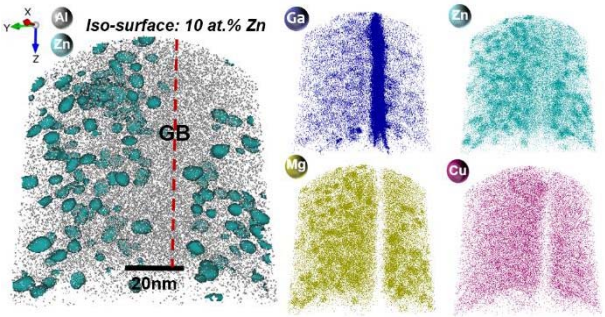

Fig. 2. APT analysis of a high-angle GB from a peak aged Al-Zn-Mg-Cu alloy prepared on a Ga-FIB, showing atom maps of the solutes and Ga.

The recent development of a FEI Helios Plasma focused ion beam (PFIB) using of alternative Xe source can alleviate this limitation. Fig. 3 is one example of the same

peak aged material prepared by Xe-FIB and analyzed by APT. The GB is clearly visible in the atom maps with a region enriched with coarse precipitates as indicated by the red rectangle. The ions of Xe in the range of the corresponding mass spectrum are also displayed, with no enrichment of Xe observed at the GB [32].

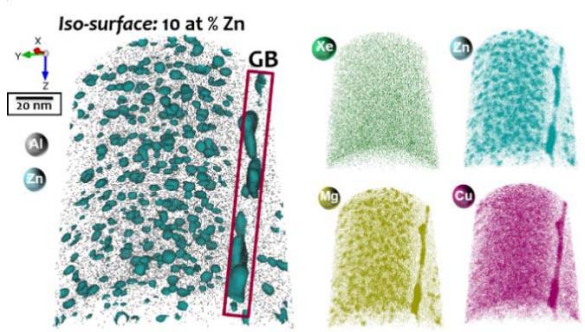

Fig. 3. APT reconstruction containing a high angle GB from a peak aged Al-Zn-Mg-Cu alloy prepared by PFIB.

3 Segregation and the early stage of precipitation at grain boundaries

Fig. 4 is an APT analysis of a high angle GB in the as-quenched Al-Zn-Mg-Cu alloy after solutionized at 475 ºC. EBSD map (Fig. 4(a)) represents the GB where several APT samples were prepared. EBSD map (Fig. 4(a)) represents the GB where several APT samples were prepared. The density map in Fig. 4(b) shows the projection of the APT dataset. The {111} poles of two adjacent grains are indexed evidencing the existence of a GB in the analyzed APT dataset. Fig. 4(c) shows the atom maps of Al, Zn, Mg, and Cu, with the GB highlighted in terms of the solute enriched. We conducted GB composition analysis by adding a cylinder across the GB and the composition profile is shown in Fig. 4(d). The result shows that Zn, Mg, and Cu segregate to the GB with an enrichment factor of approximately 2. This evidences that all solute elements segregate to the GB already after quenching and provides quantitative evidence that solutes exhibit a strong tendency to be attracted to GBs.

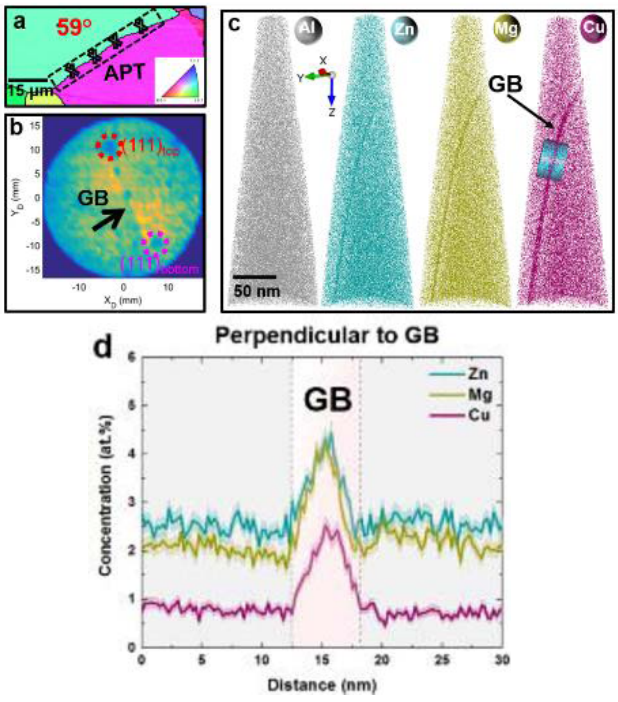

Fig. 4. APT analysis of the as-quenched Al-Zn-Mg-Cu alloy: (a) EBSD map showing the GB where APT tips were prepared; (b) Density map showing indexed crystallographic poles of the top and bottom grains; (c) Atom maps of all elements; (d) Composition profile across the GB.

Fig. 5 presents the APT analysis of the Al-Zn-Mg-Cu alloy after aging for 0.5 hours at 120°C. Nano-sized clusters are visualized by iso-surfaces of 6 at. % Zn. The GB is observed edge-on in Fig. 5(a), shown by the larger precipitate enriched region as indicated by the red arrow. Spherical Zn-Mg enriched precipitates are clearly revealed within the GB plane in Fig. 5(b). The precipitates formed within the GB are around 5 nm in size, i.e. larger than the zones with 3 nm in size distributed in the bulk. The composition profile across one GB precipitate (Fig. 5(c)) shows that it contains 60 at.% Al, 20 at.% Zn, 18 at.% Mg and 2 at.% Cu, which is close to the composition expected for GP zones ($Al_2ZnMgCu$) [6, 12, 33-36]. Typical precipitate-free zones with 10 nm in size concurrently form adjacent to the GB when the GP zones become visible, as indicated by the purple lines in Fig. 5(a). A corresponding composition profile taken across the GB in Fig. 5(d) in the region between the precipitates reveals that the solute content of Zn and Mg is about 1.5 at.% within the PFZs, which is lower than grain interior far away from the GB. This observation indicates that we do not only observe coarse precipitate formation on the GB but also solute depletion in the PFZs in the early stage aging. We observed the aging process at 120 ºC for different time and hence propose that the solute enrichments at GBs not only accelerate the formation, but also the growth and coarsening of the GB precipitates [37]. Similar accelerated precipitation behavior of Mg-Zn rich phase was also observed at the Zr-dispersoids in the same alloy [38]. The difference in the precipitate composition between the bulk and GBs was further considered and their relationship with the corrosion properties of this alloy was discussed in our recent study [39].

3.4 Interplay of segregation and local structure at GBs

We recently reported on the interplay of chemistry and faceting at GBs in the same Al-Zn-Mg-Cu alloy [40] . The GBs show significant different segregation and precipitation behavior along the GB plane. Analysis of one of the APT measurements in the as-quenched alloy is shown here in Fig. 6. The location of the GB is highlighted, with a red box in Fig. 6(a), while iso-surfaces of 5 at.% Zn+Mg are shown in Fig. 6(b) for the cross-sectional slice from this region. Fig. 6(a) demonstrates that all solute species, i.e. Zn, Mg, and Cu, have already segregated to the GB after quenching. We see in Fig. 6(b) that this segregation follows periodic patterns throughout the entire GB. These segregation patterns are formed due to the preferential segregation of Zn and Mg to particular sites. The corresponding composition profile along the

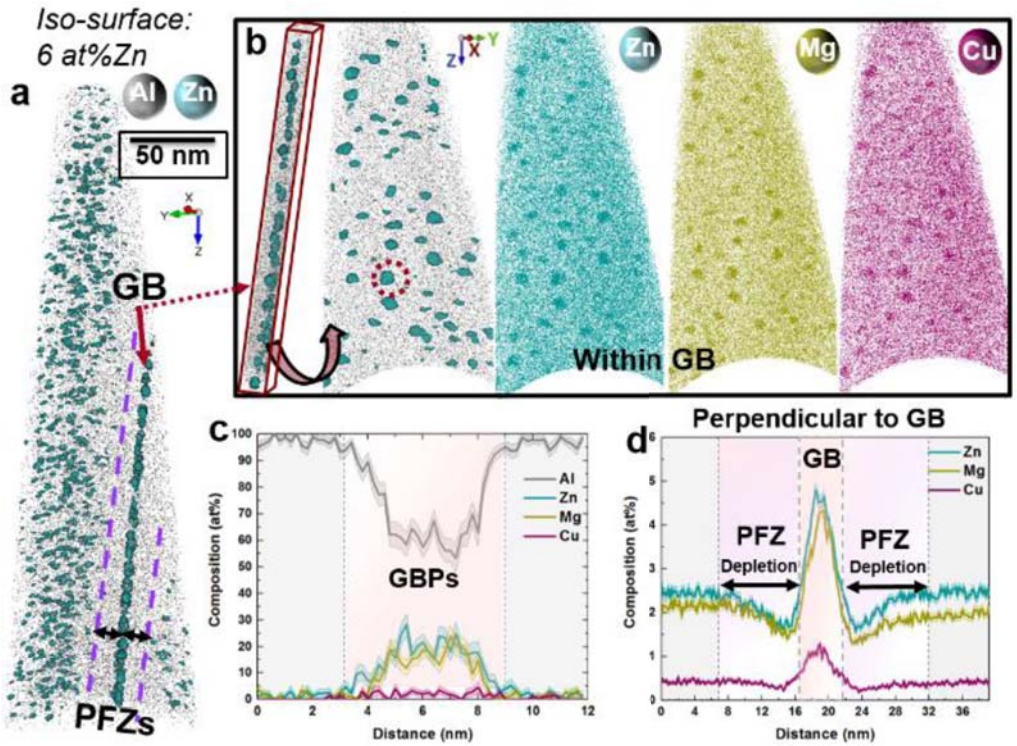

Fig. 5. APT analysis after aging for 0.5 hours at 120°C. (a) Precipitates visualized by iso-composition surfaces of 6 at% Zn; (b) Distribution of solutes along the GB plane; (c) 1D composition profile of the selected GB precipitate as indicated by the red circle; (d) 1D composition profile across the GB, devoid of GB precipitates. (Reprinted with permission from Ref. 37).

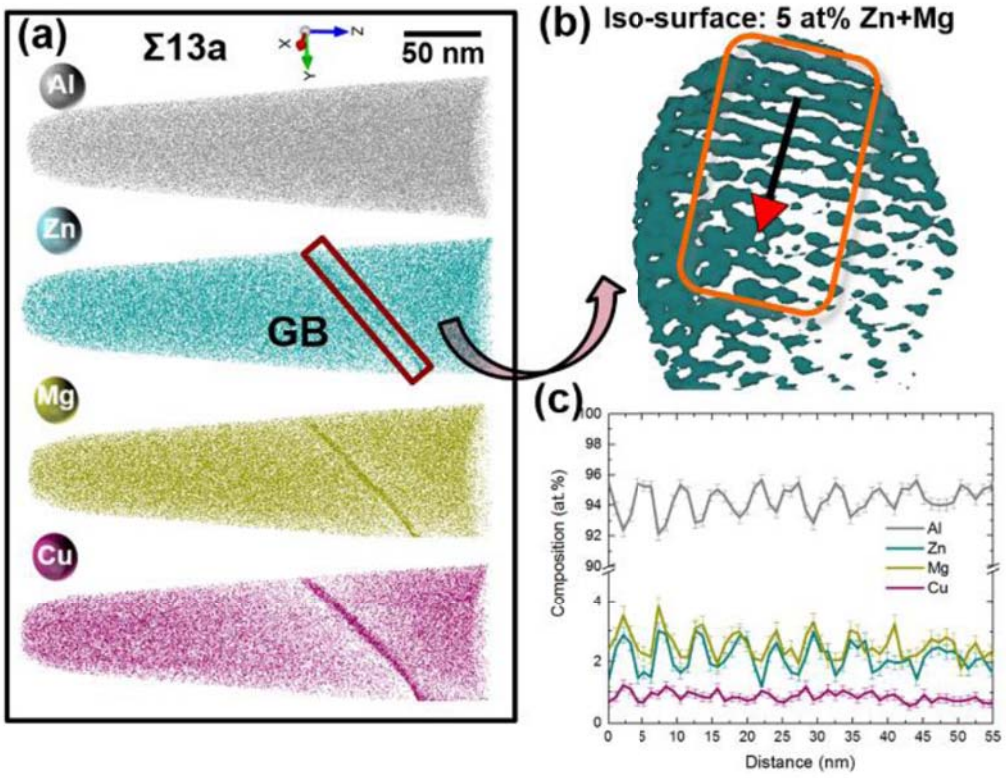

Fig. 6. (a) Atom maps of all elements of a Σ13a <110> GB in the as-quenched Al-Zn-Mg-Cu alloy; (b) Distribution of solutes within the GB plane (region indicated by the red rectangle in (a)); (c) Corresponding one-dimensional composition profile along the arrow in (b). (The Figure was reproduced from Ref. 40, for which is under the terms of the CC-Attribution 4.0 international license)

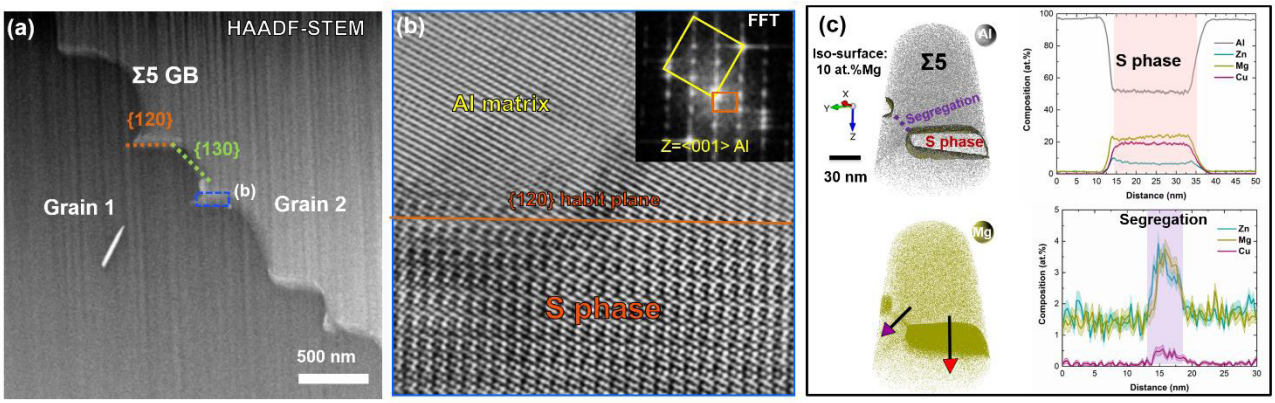

Fig. 7. (a) HAADF-STEM image of a Σ5 GB in the as-quenched Al-Zn-Mg-Cu alloy; (b) HAADF-STEM image of the precipitate highlighted by blue rectangle in (a), with inset the corresponding Fast Fourier transform (FFT) pattern; (c) APT analysis of the same GB on another location. The profiles showing the composition of the Mg-Cu enriched precipitates at the {120} facet, and the segregation at the {130} facet. (The Figure was reproduced from Ref. 40, for which is under the terms of the CC-Attribution 4.0 international license)

pattern axis is shown in Fig. 6(c). A periodic distribution is revealed, with 5 nm distance between the peaks. We revealed the interplay between the faceting and their chemical decoration with solutes at the Σ11 GB in the same alloy after solution heat treatment. The atom probe analysis shows that Mg and Zn follow similar periodic segregation patterns across the Σ11 GB plane, with a period of 6–10 nm. {200} and {111} facets alternating along the Σ11 GB were viewed by scanning transmission electron microscopy. The observed periodic patterns in the Σ13 GB might form due to the preferential segregation of Zn and Mg to particular facets, as indicated by our similar observations on the Σ11 GB. The linear segregation pattern along the GB plane is expected to affect the early stage of precipitation behavior during the subsequent aging.

Fig. 7(a) illustrates another investigation on a Σ5 GB in the as-quenched Al-Zn-Mg-Cu alloy. The GB was characterized by Z-contrast high-angle annular dark field images (HAADF)-STEM performed along the common tilt $<001>_{Al}$ zone axis. The GB configuration contains two sets of alternating facets along the entire length, with each facet highlighted by a colored dashed line in Fig. 7(a). The horizontal segments are symmetric {120} facets, and the other segments (in green) are asymmetric with a GB plane of {130}. The {120} facets bear roughly 300 nm lath-like precipitates. HAADF-STEM in Fig. 7(b) reveals that the precipitate has an orthorhombic crystal structure belonging to the cmcm group. It matches the structure of the S phase (Al_2CuMg) proposed by Perlitz and Westgren (PW model). It has an orientation relationship of $<100>_S//<100>_{Al}$, and an interface of $\{001\}_S//\{120\}_{Al}$ [41]. We performed APT analysis on the same Σ5 GB on another location, with the result shown in Fig.7(c). Two lathlike S phases enriched in Mg and Cu are visible on the {120} facets. APT crystallography analysis confirms that the habit plane of the S phase is the $\{120\}_{Al}$, which is consistent with the STEM observations. The composition profile across the S phase shows that approx. 23 at. % Mg, 18 at. % Cu, and 7 at. % Zn is enriched within the precipitate. We also observe Zn, Mg and Cu enrichment along the {130} grain boundary facets with the composition of 4 at.%, 4 at.% and, 0.5 at.% respectively. Previous studies on Al-Zn-Mg-Cu alloys showed that the S-phase can form on GBs during quenching, and the volume of the precipitates increases with decreasing cooling rates [42-45]. Investigations on Al-Cu-Mg alloys show that the S-phase forms laths on the $\{120\}_{Al}$ planes of the Σ5 GB , as its atomic arrangement in the {001} planes is identical to that on the $\{120\}_{Al}$ planes [41, 46]. Hence, it is reasonable to consider that S-phase preferentially heterogeneously nucleates at {120} facets rather than the {130} facets, which ensures good coherency and low free energy of interfaces.

4 Conclusions

In summary, we have reviewed our recent work in the application of atom probe, in conjunction with Xe-Focused Ion Beam, and electron microscopy to study the segregation and precipitation behavior in an Al-Zn-Mg-Cu alloy. We investigated the material from the solution heat treated state (475 °C), through the very early stages of aging to the peak aged state at 120 °C and further into the overaged regime at 180 °C. The process starts with solute enrichment on grain boundaries, the formation of GP zones in the solute-enriched grain boundary regions, and GP zones growth and transformation. The segregation of solutes to grain boundaries might accelerate the precipitation sequence during aging compared to the bulk. Segregation and precipitation are also strongly correlated with the local structures of GBs, which can cause the anisotropic segregation and preferential precipitation. The inhomogeneous distribution of the GB solutes can eventually reduce the GB cohesion, cause intergranular fracture, and affect the corrosion resistance of this alloy.

References

[1] E. Starke Jr, J. Staley, Progress in Aerospace Sciences, **32,** 131-172, (1996)

[2] L.F. Mondolfo, Aluminum alloys: structure and properties, Elsevier,2013.
[3] I. Polmear, Materials forum, 1-14, (2004)
[4] J.H. Chen, E. Costan, M.A. van Huis, Q. Xu, H.W. Zandbergen, Science, **312**, 416-419,(2006).
[5] L. Berg, J. Gjønnes, V. Hansen, X. Li, M. Knutson-Wedel, G. Waterloo, D. Schryvers, L. Wallenberg, Acta materialia, **49** (2001) 3443-3451.
[6] G. Sha, A. Cerezo, Acta Materialia, **52,** 4503-4516, (2004).
[7] T. Marlaud, A. Deschamps, F. Bley, W. Lefebvre, B. Baroux, Acta Materialia, **58** (2010) 4814-4826.
[8] A. Guinier, Nature, **142,** 569, (1938)
[9] G.D. Preston, The London, Edinburgh, and Dublin Philosophical Magazine and Journal of Science, **26,** 855-871, (2009)
[10] F. Cao, J. Zheng, Y. Jiang, B. Chen, Y. Wang, T. Hu, Acta Materialia, **164**, 207-219, (2019)
[11] X. Li, V. Hansen, J. Gjønnes, L. Wallenberg, Acta materialia, **47**, 2651-2659, (1999)
[12] K. Hono, N. Sano, T. Sakurai, Surface science, **266**,350-357, (1992)
[13] T. Marlaud, A. Deschamps, F. Bley, W. Lefebvre, B. Baroux, Acta Materialia, **58**, 248-260, (2010)
[14] A. Deschamps, Y. Bréchet, Materials Science and Engineering: A, **251**, 200-207, (1998)
[15] Y. Komura, K. Tokunaga, Acta Crystallographica Section B: Structural Crystallography and Crystal Chemistry, **36**,1548-1554, (1980)
[16] J. Gjønnes, C.J. Simensen, Acta Metallurgica, **18**,881-890, (1970)
[17] S.P. Knight, N. Birbilis, B.C. Muddle, A.R. Trueman, S.P. Lynch, Corrosion Science, **52** 4073-4080, (2010)
[18] R.M. Su, Y.D. Qu, R.D. Li, J.H. You, Materials Science, **51**, 372-380, (2015)
[19] A.C.U. Rao, V. Vasu, M. Govindaraju, K.V.S. Srinadh, Transactions of Nonferrous Metals Society of China, **26**, 1447-1471, (2016)
[20] P. Pao, M. Gao, R. Wei, Scripta metallurgica, **19** 265-270, (1985)
[21] A. Joshi, C. Shastry, M. Levy, Metallurgical Transactions A, **12**, 1081-1088, (1981)
[22] R. Viswanadham, T. Sun, J. Green, Metallurgical and Materials Transactions A, **11**, 85-89, (1980)
[23] A.K. Vasudevan, R. Doherty, Acta metallurgica, **35**, 1193-1219, (1987)
[24] T. Ogura, S. Hirosawa, A. Cerezo, T. Sato, Acta Materialia, **58**, 5714-5723, (2010).
[25] E.A. Starke, JOM, **22**, 54-63, (1970)
[26] D. Raabe, M. Herbig, S. Sandlöbes, Y. Li, D. Tytko, M. Kuzmina, D. Ponge, P.P. Choi, Current Opinion in Solid State and Materials Science, **18**, 253-261, (2014)
[27] T. Frolov, S.V. Divinski, M. Asta, Y. Mishin, Physical review letters, **110**, 255502, (2013)
[28] M. Kuzmina, D. Ponge, D. Raabe, Acta Materialia, **86**, 182-192, (2015)
[29] M.P. Harmer, Science, **332**, 182-183, (2011)
[30] P. Lejcek, Springer series in materials science, **136**, (2010)
[31] H. Zhao, B. Gault, D. Ponge, D. Raabe, F. De Geuser, Scripta Materialia, **154**, 106-110, (2018).
[32] Y. Xiao, J. Wehrs, H. Ma, T. Al-Samman, S. Korte-Kerzel, M. Göken, J. Michler, R. Spolenak, J.M. Wheeler, Scripta Materialia, **127**, 191-194, (2017).
[33] S. Ringer, K. Hono, Materials characterization, **44**, 101-131, (2000)
[34] P.V. Liddicoat, T. Honma, L.T. Stephenson, S.P. Ringer, Materials Science Forum, **519-521,** 555-560, (2006)
[35] T. Engdahl, V. Hansen, P. Warren, K. Stiller, Materials Science and Engineering: A, **327** 59-64, (2002)
[36] C. Wolverton, Acta Materialia, **49**, 3129-3142, (2001)
[37] H. Zhao, F. De Geuser, A. Kwiatkowski da Silva, A. Szczepaniak, B. Gault, D. Ponge, D. Raabe, Acta Materialia, **156**, 318-329, (2018)
[38] H. Zhao, Y. Chen, B. Gault, S.K. Makineni, D. Ponge, D. Raabe, Materialia, **10**, (2020)
[39] H. Zhao, B. Gault, D. Ponge, D. Raabe, Scripta Materialia, **188**, 269-273, (2020)
[40] H. Zhao, L. Huber, W. Lu, N.J. Peter, D. An, F. De Geuser, G. Dehm, D. Ponge, J. Neugebauer, B. Gault, D. Raabe, Phys Rev Lett, **124**, 106102, (2020)
[41] V. Radmilovic, R. Kilaas, U. Dahmen, G. Shiflet, Acta Materialia, 47, 3987-3997, (1999)
[42] Y. Zhang, B. Milkereit, O. Kessler, C. Schick, P.A. Rometsch, Journal of Alloys and Compounds, **584**, 581-589, (2014)
[43] B. Yang, B. Milkereit, Y. Zhang, P.A. Rometsch, O. Kessler, C. Schick, Materials Characterization, **120**, 30-37,(2016)
[44] D. Godard, P. Archambault, E. Aeby-Gautier, G. Lapasset, Acta Materialia, 50 (2002) 2319-2329.
[45] C. Mondal, A.K. Mukhopadhyay, Materials Science and Engineering: A, **391**, 367-376. (2005)
[46] G.B. Winkelman, K. Raviprasad, B.C. Muddle, Acta Materialia, **55**, 3213-3228, (2007)